Simulation of long eccentricity (400-kyr) cycle in ocean carbon reservoir during Miocene Climate Optimum: Weathering and nutrient response to orbital change

Wentao Ma,[1] Jun Tian,[1] Qianyu Li,[1,2] and Pinxian Wang[1]

Received 6 April 2011; accepted 10 April 2011; published 20 May 2011.

[1] Deep-sea foraminiferal $\delta^{13}C$ records contain abundant 400-kyr cycles indicating a link between eccentricity forcing and ocean carbon reservoir change. Here we simulate the oceanic $\delta^{13}C$ maxima events forced by the Earth's orbital geometry during the Miocene Climate Optimum (MCO, 17-14 Ma) using a box model. The simulated results of both surface and deep water $\delta^{13}C$ display co-varying 400-kyr cycle. Modulated by orbital parameters, weathering induced carbon input will change the burial ratio of carbonates to organic carbon and further result in periodic changes in the oceanic $\delta^{13}C$. The increase of riverine nutrient input, which is synchronous with riverine carbon input, often stimulates primary productivity and burial of organic carbon. Our results support that eccentricity maxima (minima) enhance (reduce) weathering intensity and nutrient supply, which lead to minima (maxima) of $\delta^{13}C$. The prominent 400-kyr cycle of ocean carbon reservoir is interpreted as likely caused by a long memory of carbon in the ocean. **Citation:** Ma, W., J. Tian, Q. Li, and P. Wang (2011), Simulation of long eccentricity (400-kyr) cycle in ocean carbon reservoir during Miocene Climate Optimum: Weathering and nutrient response to orbital change, *Geophys. Res. Lett.*, *38*, L10701, doi:10.1029/2011GL047680.

1. Introduction

[2] The 400-kyr cycle in foraminiferal carbon isotopes ($\delta^{13}C$), which is related to the Earth's long eccentricity, exists not only in the Pliocene records [*Wang et al.*, 2010, and references therein] but also in the Oligocene [*Pälike et al.*, 2006; *Wade and Pälike*, 2004] and the Miocene [*Woodruff and Savin*, 1991; *Holbourn et al.*, 2007]. These 400-kyr cycles often perform as a series of $\delta^{13}C$ maxima that correspond to long eccentricity's minima and some important cooling events (e.g., Oi-1 and Mi-1 as [*Miller et al.*, 1991]) during the late Cenozoic [*Wang et al.*, 2010]. This long eccentricity paced cycle, which has been considered as one component of the "heartbeat" of the Earth's climate system [*Pälike et al.*, 2006], is thus crucial to predict future long term trend of climate change.

[3] In contrast to the well preserved 400-kyr cycle in a "hothouse" or small ice sheet world [*Cramer et al.*, 2003; *Pälike et al.*, 2006], the long eccentricity cycle in late Pleistocene $\delta^{13}C$ records from global oceans was obscured by extending to ~500-kyr with a relatively weaker amplitude [*Wang et al.*, 2004; 2010]. The expansion of large ice sheets during the late Pleistocene may have produced this cycle change by suppressing the 400-kyr cycle in the ocean carbon reservoir [see also *Wang et al.*, 2010].

[4] Compared with the late Pleistocene, the Miocene climate optimum (MCO, 17-14 Ma) is a warm period with limited influences from a small Eastern Antarctic Ice Sheet [*Flower and Kennett*, 1994]. The MCO is also characterized by a series of carbon isotope maxima events (CM events) which are paced by 400-kyr cycle [*Woodruff and Savin*, 1991; *Holbourn et al.*, 2007] and thus is a more suitable period for simulating the 400-kyr cycle in climate variability.

[5] In this paper, we simulate the CM events during the MCO using a box model forced by Earth's orbital variations to test the effects of burial of organic carbon and $CaCO_3$ on the periodical changes in the ocean carbon reservoir.

2. Model Description

[6] We use box model, a good choice for long time series simulations [e.g., *Pälike et al.*, 2006], to simulate the 400-kyr variability of oceanic $\delta^{13}C$. Our box model contains 6 oceanic boxes and one atmospheric box (Figure 1). The configuration of ocean-atmosphere system follows the division by *Lane et al.* [2006], which contain the minimum number of boxes that can capture the major ocean circulation. Surface ocean is divided by 45° S/N into 3 boxes, a southern box "S", an equatorial box "E" and a northern box "N". Three deeper ocean boxes include a northern deep box "D", a southern intermediate box "I", and a bottom box "B". Variables in each oceanic box include phosphate, dissolved inorganic carbon (DIC), alkalinity (ALK) and $\delta^{13}C$. We follow the biogeochemical calculation used by *Toggweiler* [2008] but make some minor modifications. The atmospheric box receives volcano and kerogene degassing of CO_2. Surface box receives riverine inputs of DIC and ALK due to the weathering of carbonate and silicate rocks. Wsil and Wcar are weathering rates for silicate and carbonate rocks, respectively. The phosphate level is taken as the limit nutrient for the primary productivity (PP). We remove carbon from the system in the form of burial of $CaCO_3$ and organic matter but carbon can also enter the system through dissolution of $CaCO_3$ other than riverine inputs. More details about the model are given in the auxiliary material.[1]

[7] The box model is externally forced by variations in ETP between 17 and 13 Ma based on an astronomical

[1]State Key Laboratory of Marine Geology, Tongji University, Shanghai, China.
[2]School of Earth and Environmental Sciences, University of Adelaide, Adelaide, South Australia, Australia.

0094-8276/11/2011GL047680

[1]Auxiliary materials are available in the HTML. doi:10.1029/2011GL047680.

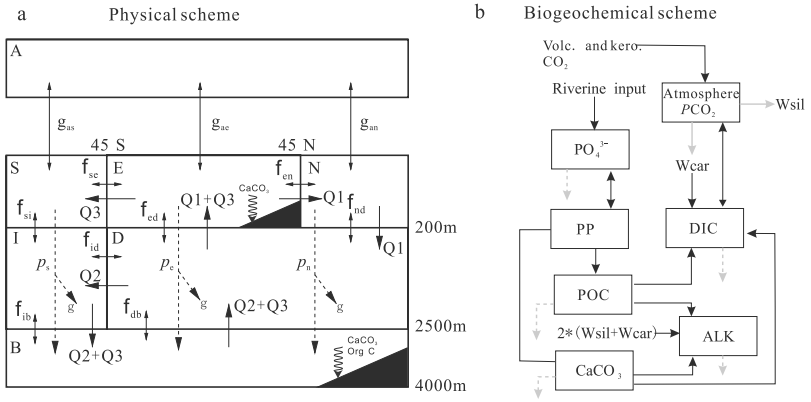

Figure 1. Configuration of the box model. (a) Physical scheme. (b) Biogeochemical scheme. See detailed description in text and the auxiliary material.

solution of La2004 [*Laskar et al.*, 2004]. ETP is the sum of normalized eccentricity, obliquity and precession in a ratio of 1:1:−1.

3. Results and Discussion

3.1. Simulated $\delta^{13}C$ Results Under Weathering and Nutrient Supply Scenarios

[8] We run the model from the initial state for 2 million years until it reaches an equilibrium state (Tables S2 and S3 of the auxiliary material). Then, the model is spun up by modifying specific parameters to investigate their significant levels in the resulted variability of $\delta^{13}C$. We design three specific tests as shown below.

[9] 1) Weathering test. The riverine inputs of DIC and ALK are forced using equations Wsil = $5.0 \times 10^{12} \times (1 + 0.15 \times \mathrm{ETP})$ mol/yr and Wcar = $10.7 \times 10^{12} \times (1 + 0.3 \times \mathrm{ETP})$ mol/yr, respectively, while the input of phosphate is kept constant.

[10] 2) Phosphate input test. The riverine input of phosphate is forced using the equation $\mathrm{rivPO_4} = 5.0 \times 10^{12} \times (1 + 0.3 \times \mathrm{ETP})/200$ mol/yr, while the riverine inputs of carbon are kept constant.

[11] 3) Integrated test. The weathering inputs from silicates and carbonates are forced, respectively, using equations Wsil = $5.0 \times 10^{12} \times (1 + 0.15 \times \mathrm{ETP})$ mol/yr and Wcar = $10.7 \times 10^{12} \times (1 + 0.3 \times \mathrm{ETP})$ mol/yr, while the input of phosphate is forced using $\mathrm{rivPO_4}$ = Wsil/200 mol/yr. The burial of shallow water carbonates is forced by *Carbsh* = $9 \times 10^{12} \times (1 + \mathrm{ETP})$ mol/yr.

[12] In each test, the riverine inputs of DIC, ALK and nutrient supply are changed as a function of ETP to evaluate effects of burial of $CaCO_3$ and organic carbon on oceanic $\delta^{13}C$. The equations given above implicitly assume that weathering and nutrient inputs linearly respond to orbital parameter changes [e.g., *Pälike et al.*, 2006], although the detailed physical mechanisms are not yet clear.

[13] Simulated $\delta^{13}C$ results from the "integrated test" (Figure 2) and the other two tests (Figures S1 and S2 of the auxiliary material) show very strong and stable 400-kyr cycle (Figure S3) relative to the 100-kyr, 40-kyr, 23-kyr and 19-kyr cycle, which is different from the nearly equal power at the eccentricity, obliquity and precession bands from the external forcing (ETP). The simulated $\delta^{13}C$ of bottom water ($\delta^{13}C_{bottom}$) shows a great resemblance to the benthic foraminiferal $\delta^{13}C$ record from Ocean Drilling Program (ODP) Site 1237 [*Holbourn et al.*, 2007] (Figure 3b). In general, the simulated $\delta^{13}C$ of surface water ($\delta^{13}C_{surface}$) mimics the actual record of $\delta^{13}C_{benthic}$ Comparison with planktonic $\delta^{13}C$ is not feasible because high resolution actual $\delta^{13}C_{planktonic}$ records are lacking. The $\delta^{13}C$ outputs of the "integrated test" are similar with the "weathering test", indicating that riverine inputs of DIC and ALK play the most important role in modulating the $\delta^{13}C$ (Figure 3a). The synchronous riverine nutrient inputs, as in the "phosphate input test" and "integrated test", will stimulate primary productivity and burial of organic carbon when eccentricity is at high amplitude. Some mismatches between the simulated $\delta^{13}C$ and the benthic foraminiferal $\delta^{13}C$ of ODP Site 1237 start to occur after 13.5 Ma (Figure 3b). This discrepancy can attribute to the expansion of Eastern Antarctic Ice Sheet during the middle Miocene which alters boundary condition during that period and thus causes the benthic $\delta^{13}C$ changes [e.g., *Tian et al.*, 2009]. As our model focuses on an ice-free world, the effects of ice sheet expansion on oceanic $\delta^{13}C$ will have to be evaluated in later studies.

3.2. The 400-kyr Cycle of Simulated $\delta^{13}C$ and Phase Relationship With Eccentricity

[14] The augment of the 400-kyr cycle in simulated $\delta^{13}C$ is probably due to the long memory effects of carbon in the ocean [*Broecker and Peng*, 1982]. In our model, the residence time of carbon in ocean-atmosphere system, calculated through standing carbon stock divided by burial rate of carbon as definition, is ~135 kyrs when the system reaches static state, which is consistent with the assumption that an order of 10^5 years is required for the carbon residence time [*Cramer et al.*, 2003].

[15] The "integrated test" demonstrates that the simulated $\delta^{13}C_{bottom}$ and $\delta^{13}C_{surface}$ maxima correspond to the minima of eccentricity, burial of organic carbon and total $CaCO_3$ (Figure 2). The terms "maxima" and "minima" at the 400-kyr band are used to refer to the peak and trough values, respectively, in the following discussion. The anti-phase relationship between the simulated $\delta^{13}C$ and the burial ratio of total $CaCO_3$ to organic carbon in the "integrated test" (Figure 2) and "weathering test" (Figure S1) agrees well with the result from *Cramer et al.* [2003], indicating that a net decrease of burial of $CaCO_3$ in relation to organic carbon will lead to an increase in the $\delta^{13}C$ and that the burial ratio of

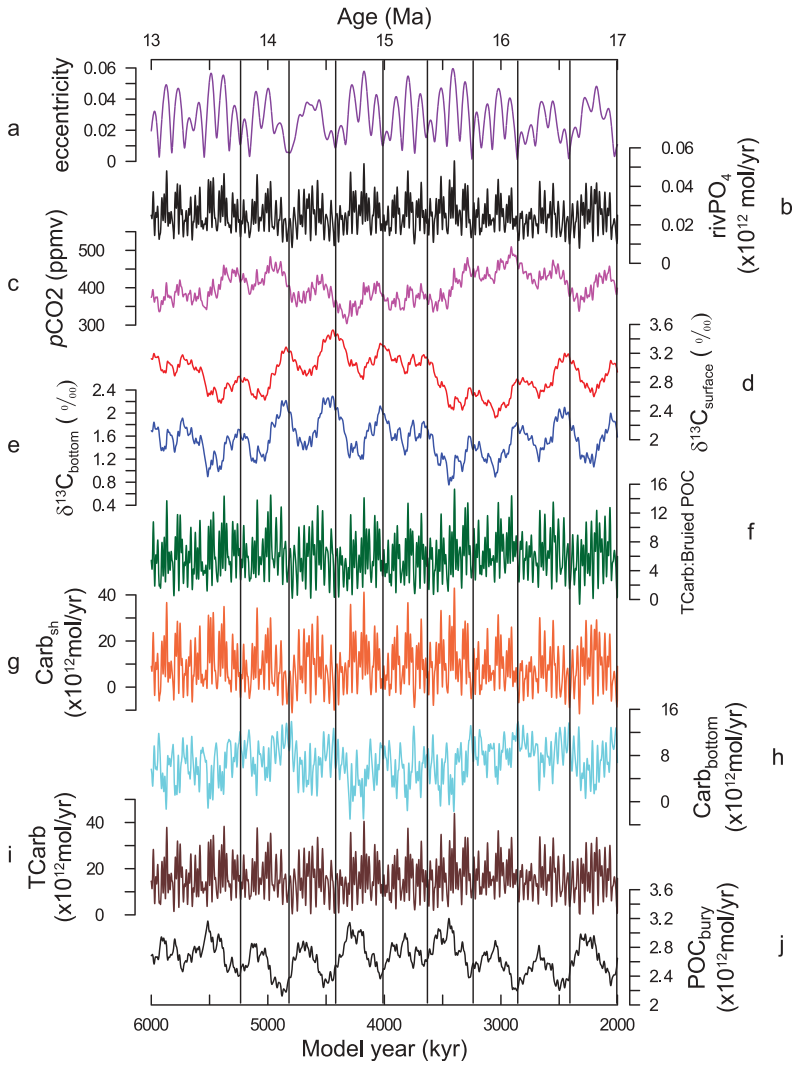

Figure 2. Simulated results of the "integrated test". (a) Eccentricity of the Earth from La2004 solution [*Laskar et al.*, 2004]; (b) riverine phosphate input as external forcing; (c) concentration of atmospheric CO_2; (d) averaged $\delta^{13}C$ in boxes "S", "E" and "N"; (e) $\delta^{13}C$ in box "B"; (f) burial ratio of total $CaCO_3$ to POC; (g) burial of $CaCO_3$ in box "E"; (h) burial of $CaCO_3$ in box "B"; (i) burial of total $CaCO_3$ in boxes "E" and "B"; (j) burial of organic carbon. The top x axis denotes the geological age while the bottom x axis denotes the time that model runs from the reference time of 0.

$CaCO_3$ to organic carbon is a key factor controlling the oceanic $\delta^{13}C$. The phases of $\delta^{13}C_{bottom}$ and $\delta^{13}C_{surface}$ are consistent in the "weathering test", indicating that the burial of $CaCO_3$ affects the carbon isotope of the whole water column. In the "phosphate input test", $\delta^{13}C_{surface}$ leads $\delta^{13}C_{bottom}$ by 40–70 kyrs, probably due to the remineralization of organic carbon. Organic carbon raises $\delta^{13}C_{surface}$ as being exported and lowers $\delta^{13}C_{bottom}$ as being remineralized. The planktonic $\delta^{13}C$ generally mimic the benthic $\delta^{13}C$ in geological records [e.g., *Woodruff and Savin*, 1991; *Zhao et al.*, 2001], indicating a link between them. Our simulation results also support that riverine inputs of weathering DIC and ALK cause significant change in the ocean carbon reservoir (including $CaCO_3$ and $\delta^{13}C$). The riverine nutrient input alone, however, does not produce consistent changes between $\delta^{13}C_{surface}$ and $\delta^{13}C_{bottom}$.

3.3. Sedimentation of Carbonates During the MCO

[16] In geological records, the variability of foraminiferal $\delta^{13}C$ also corresponds to the dissolution/preservation of $CaCO_3$ in 400-kyr band, that when eccentricity is in maximum (minimum), $CaCO_3$ is less (well) preserved and $\delta^{13}C$ is lighter (heavier) [*Flower and Kennett*, 1994; *Holbourn et al.*, 2007]. *Holbourn et al.* [2007] proposed that the dissolution of $CaCO_3$ during eccentricity maxima is probably owing to the redistribution of its burial between shallow and bottom water. The strong monsoons in eccentricity's maximum durations enhance the burial of $CaCO_3$ in tropical shallow seas at the expanse of that is buried in deep water, resulting in depletion of $\delta^{13}C$ and release of CO_2 to the atmosphere [*Holbourn et al.*, 2007]. Based on the above hypothesis, we force the burial of shallow water $CaCO_3$ in the simulation experiment by ETP parameters. The simulated burial of shallow water $CaCO_3$ (Figure 2g) and total $CaCO_3$ (Figure 2i) increase during eccentricity maxima but displays anti-phase relationship with the burial of $CaCO_3$ in bottom water (Figure 2h). The simulated concentration of atmospheric CO_2 (pCO_2) (Figure 2c) shows in-phase relationship with the burial of shallow water and total $CaCO_3$. Our simulated results support that the burial of $CaCO_3$

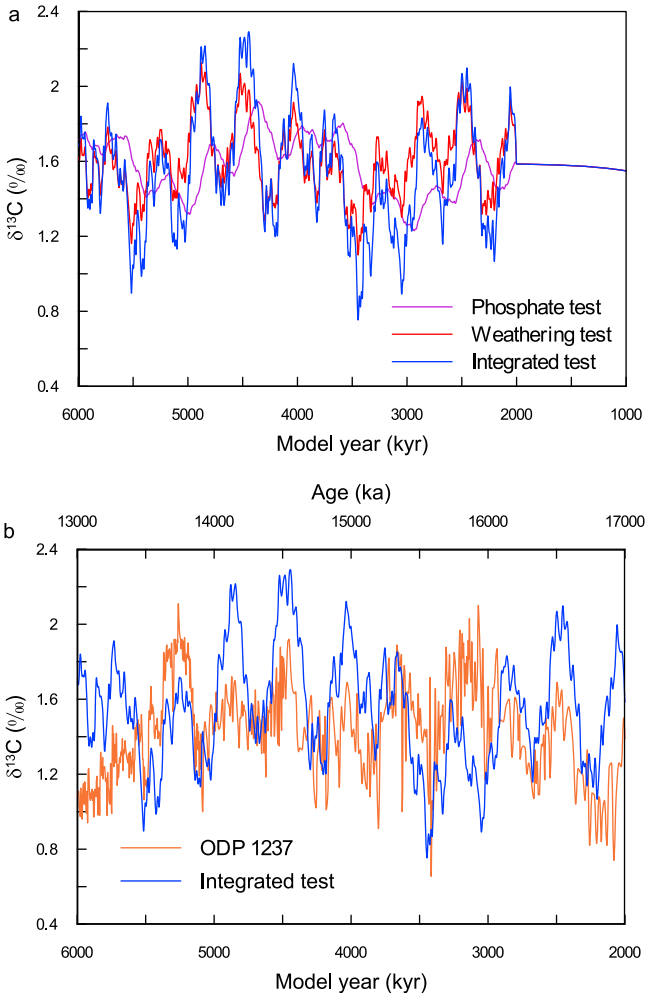

Figure 3. (a) Amplitude comparison of carbon isotopes of box "B" between three different tests; (b) comparison of carbon isotopes of box "B" in the "integrated test" to the benthic δ^{13}C record from ODP Site 1237 [*Holbourn et al.*, 2007].

increased but mainly in the form of shallow water carbonates during MCO when eccentricity is in maximum. Accordingly, the lysocline shoals or deepens when eccentricity is in maximum or minimum. Simulated pCO_2 is consistent with findings that sea-level is low (high) as a result of the cooling (warming) effect of low (hingh) pCO_2 when eccentricity is in maximum (minimum) [*Flower and Kennett*, 1994].

3.4. Long Eccentricity Forcing of the Carbon Isotope Maxima Events During the MCO

[17] Humid climate conditions favoring chemical weathering during the MCO have been revealed in oxygen isotopic records [*Kaandorp et al.*, 2005]. High weathering fluxes from the Asian continent are transported to the low latitude Pacific and Indian oceans during that time [*Clift*, 2006; *Wan et al.*, 2009]. In low latitude regions, monsoon is a dominant factor affecting the extent of weathering [*Clift and Plumb*, 2008]. The orbital scale variability of monsoon exhibits dominant precession cycles [*Kutzbach*, 1981; *Wang*, 2009], but the amplitude variation of precession cycles is controlled by the eccentricity. Often, higher eccentricity results in bigger amplitude of the climate precession and hence larger wet/dry variations in tropics [*Ruddiman*, 2008]. Larger dry/wet variability will causes stronger physical and chemical weathering which produces more fine-grain materials to be transported as sediments and nutrient. An opposite scenario will occur at low eccentricity when a hyperarid climate may prevail [*Hovan and Rea*, 1992, and references therein]. Therefore, if a monsoon-dominated climate system was already established in the Miocene [*Guo et al.*, 2008], a strong weathering intensity during the MCO would be controlled by eccentricity modulated monsoon maxima, which must have contributed greatly to the long eccentricity cycle in the ocean carbon reservoir. Therefore, the widely distributed CM events in global oceans [*Woodruff and Savin*, 1991; *Holbourn et al.*, 2007], can attribute to strong weathering and high riverine nutrient supply to the ocean during the MCO. Our model experiments explicitly reveal that the ETP takes a major role as a primary external forcing in triggering the 400-kyr cycle in the ocean carbon reservoir changes. Changes in weathering and riverine carbon supply are most important feedbacks internal to the Earth system during the MCO to produce such long eccentricity cycle widely found in δ^{13}C records from world oceans. The synchronous riverine nutrient input is also an important factor in stimulating primary productivity and burial of organic carbon.

4. Concluding Remark

[18] The modern eccentricity of the Earth is passing through another minimum which is corresponding to the current oceanic δ^{13}C maximum. Our box model results shed light on understanding the origin of 400-kyr cycle of oceanic carbon reservoir change. The 400-kyr cycle of oceanic δ^{13}C implies the response of ocean carbon reservoir change to tropical processes.

[19] **Acknowledgments.** We are grateful to J. R. Toggweiler for providing the source code of the box model and intensive discussion during drafting of this manuscript. This research is supported by National Basic Research Program of China (grant 2007CB815902) and Natural Science Foundation of China (grants 40976024 and 41076017). Jun Tian also thanks supports from Shanghai Rising-Star Program (grant 10QH1402600), Fok Ying Tong Education Foundation (111016) and program for New Century Excellent Talents in University (NCET-08-0401).

[20] The Editor thanks Babette Hoogakker and an anonymous reviewer for their assistance in evaluating this paper.

References

Broecker, W. S., and T.-H. Peng (1982), *Tracers in the Sea*, 690 pp., Eldigio, Palisades, N. Y.

Clift, P. D. (2006), Controls on the erosion of Cenozoic Asia and the flux of clastic sediment to the ocean, *Earth Planet. Sci. Lett.*, *241*(3–4), 571–580, doi:10.1016/j.epsl.2005.11.028.

Clift, P. D., and R. A. Plumb (2008), *The Asian Monsoon: Causes, History and Effects*, 270 pp., Cambridge Univ. Press, Cambridge, U. K., doi:10.1017/CBO9780511535833.

Cramer, B. S., J. D. Wright, D. V. Kent, and M. P. Aubry (2003), Orbital climate forcing of δ^{13}C excursions in the late Paleocene-early Eocene (chrons C24n-C25n), *Paleoceanography*, *18*(4), 1097, doi:10.1029/2003PA000909.

Flower, B. P., and J. P. Kennett (1994), The middle Miocene climatic transition: East Antarctic ice sheet development, deep ocean circulation and global carbon cycling, *Palaeogeogr. Palaeoclimatol. Palaeoecol.*, *108*(3–4), 537–555, doi:10.1016/0031-0182(94)90251-8.

Guo, Z. T., et al. (2008), A major reorganization of Asian climate by the early Miocene, *Clim. Past*, *4*(3), 153–174, doi:10.5194/cp-4-153-2008.

Holbourn, A., W. Kuhnt, M. Schulz, J. A. Flores, and N. Andersen (2007), Orbitally-paced climate evolution during the middle Miocene "Monterey" carbon-isotope excursion, *Earth Planet. Sci. Lett.*, *261*(3–4), 534–550, doi:10.1016/j.epsl.2007.07.026.

Hovan, S. A., and D. A. Rea (1992), The Cenozoic record of continental mineral deposition on Broken and Ninetyeast Ridges, Indian Ocean: Southern African aridity and sediment delivery from the Himalayas, *Paleoceanography*, *7*(6), 833–860, doi:10.1029/92PA02176.

Kaandorp, R. J. G., H. B. Vonhof, F. P. Wesselingh, L. R. Pittman, D. Kroon, and J. E. van Hinte (2005), Seasonal Amazonian rainfall variation in the Miocene Climate Optimum, *Palaeogeogr. Palaeoclimatol. Palaeoecol.*, *221*(1–2), 1–6, doi:10.1016/j.palaeo.2004.12.024.

Kutzbach, J. E. (1981), Monsoon climate of the early Holocene: Climate experiment with Earth's orbital parameters for 9000 years ago, *Science*, *214*(4516), 59–61, doi:10.1126/science.214.4516.59.

Lane, E., S. Peacock, and A. M. Restrepo (2006), A dynamic-flow carbon-cycle box model and high-latitude sensitivity, *Tellus, Ser. B*, *58*(4), 257–278, doi:10.1111/j.1600-0889.2006.00192.x.

Laskar, J., P. Robutel, F. Joutel, M. Gastineau, A. C. M. Correia, and B. Levrard (2004), A long-term numerical solution for the insolation quantities of the Earth, *Astron. Astrophys.*, *428*(1), 261–285, doi:10.1051/0004-6361:20041335.

Miller, K. G., J. D. Wright, and R. G. Fairbanks (1991), Unlocking the ice house: Oligocene-Miocene oxygen isotopes, eustasy, and margin erosion, *J. Geophys. Res.*, *96*(B4), 6829–6848, doi:10.1029/90JB02015.

Pälike, H., R. D. Norris, J. O. Herrle, P. A. Wilson, H. K. Coxall, C. H. Lear, N. J. Shackleton, A. K. Tripati, and B. S. Wade (2006), The heartbeat of the oligocene climate system, *Science*, *314*(5807), 1894–1898, doi:10.1126/science.1133822.

Ruddiman, W. F. (2008), *Earth's Climate: Past and Future*, 2nd ed., 388 pp., W. H. Freeman, New York.

Tian, J., A. Shevenell, P. X. Wang, Q. H. Zhao, Q. Y. Li, and X. R. Cheng (2009), Reorganization of Pacific Deep Waters linked to middle Miocene Antarctic cryosphere expansion: A perspective from the South China Sea, *Palaeogeogr. Palaeoclimatol. Palaeoecol.*, *284*(3–4), 375–382, doi:10.1016/j.palaeo.2009.10.019.

Toggweiler, J. R. (2008), Origin of the 100,000-year timescale in Antarctic temperatures and atmospheric CO_2, *Paleoceanography*, *23*, PA2211, doi:10.1029/2006PA001405.

Wade, B. S., and H. Pälike (2004), Oligocene climate dynamics, *Paleoceanography*, *19*, PA4019, doi:10.1029/2004PA001042.

Wan, S. M., W. M. Kurschner, P. D. Clift, A. C. Li, and T. G. Li (2009), Extreme weathering/erosion during the Miocene Climatic Optimum: Evidence from sediment record in the South China Sea, *Geophys. Res. Lett.*, *36*, L19706, doi:10.1029/2009GL040279.

Wang, P. X. (2009), Global monsoon in a geological perspective, *Chin. Sci. Bull.*, *54*(7), 1113–1136, doi:10.1007/s11434-009-0169-4.

Wang, P. X., J. Tian, X. R. Cheng, C. L. Liu, and J. Xu (2004), Major Pleistocene stages in a carbon perspective: The South China Sea record and its global comparison, *Paleoceanography*, *19*, PA4005, doi:10.1029/2003PA000991.

Wang, P. X., J. Tian, and L. J. Lourens (2010), Obscuring of long eccentricity cyclicity in Pleistocene oceanic carbon isotope records, *Earth Planet. Sci. Lett.*, *290*(3–4), 319–330, doi:10.1016/j.epsl.2009.12.028.

Woodruff, F., and S. Savin (1991), Mid-Miocene isotope stratigraphy in the deep sea: High-resolution correlations, paleoclimatic cycles, and sediment preservation, *Paleoceanography*, *6*(6), 755–806, doi:10.1029/91PA02561.

Zhao, Q., P. Wang, X. Cheng, J. Wang, B. Huang, J. Xu, Z. Zhou, and Z. Jian (2001), A record of Miocene carbon excursions in the South China Sea, *Sci. China Ser. D Earth Sci.*, *44*(10), 943–951, doi:10.1007/BF02907087.

Q. Li, W. Ma, J. Tian, and P. Wang, State Key Laboratory of Marine Geology, Tongji University, Shanghai 200092, China. (8wentao_ma@tongji.edu.cn)